Comput Mech
DOI 10.1007/s00466-007-0222-6

ORIGINAL PAPER

A cohesive finite element for quasi-continua

Xiaohu Liu · Shaofan Li · Ni Sheng

Received: 18 May 2007 / Accepted: 20 September 2007

Abstract In this paper, a cohesive finite element method (FEM) is proposed for a quasi-continuum (QC), i.e. a continuum model that utilizes the information of underlying atomistic microstructures. Most cohesive laws used in conventional cohesive FEMs are based on either empirical or idealized constitutive models that do not accurately reflect the actual lattice structures. The cohesive quasi-continuum finite element method, or cohesive QC-FEM in short, is a step forward in the sense that: (1) the cohesive relation between interface traction and displacement opening is now obtained based on atomistic potentials along the interface, rather than empirical assumptions; (2) it allows the local QC method to simulate certain inhomogeneous deformation patterns. To this end, we introduce an *interface or discontinuous Cauchy–Born rule* so the interfacial cohesive laws are consistent with the surface separation kinematics as well as the atomistically enriched hyperelasticity of the solid. Therefore, one can simulate inhomogeneous or discontinuous displacement fields by using a simple local QC model. A numerical example of a screw dislocation propagation has been carried out to demonstrate the validity, efficiency, and versatility of the method.

Keywords Cohesive laws · Dislocation · Finite element method · Nano-mechanics · Quasi-continuum

1 Introduction

The numerical simulation of strong and weak discontinuities has been one of the major focuses of computational failure mechanics and engineering reliability analysis in recent years. Several finite element methods (FEMs) have been proposed. Two of the most successful methods are the cohesive FEM proposed by [17], and the so-called extended finite element method (X-FEM) proposed by Belytschko et al. [1]. However, most of these methods adopt phenomenological constitutive relations, which may not be suitable for computational nanomechanics. For example, when it comes to simulations of individual dislocation motions, we are not only interested in how a dislocation moves but also how it affects the motion of neighboring atoms. The traditional FE based methods usually have difficulties in capturing those details. An alternative method is molecular dynamics (MD), which has been successfully applied to simulations of the crack growth. However MD simulates the motion of every single atom in the domain, the computational cost can be enormous if the size of the spatial domain of the simulation is up or beyond nanoscale. Today most MD simulations of fracture are only limited in nano- or sub-nanoscales.

To build a cost-effective simulation tool, a class of so-called coarse-grained methods has been proposed. These methods exploit the information at the atomic level but retain some basic features of continuum mechanics. One of the popular coarse-grained methods is the Quasi-continuum (QC) method, e.g. [16]. A comprehensive review can be found in [12]. There are two versions of the QC method: the local QC and the non-local QC. The local version of QC method adopts the Cauchy–Born rule, and hence it can only apply to where the local deformation is uniform; while the non-local version was designed to simulate inhomogeneous local deformations. To achieve that, it needs atomic resolution, and hence it is not really a coarse grain model. Therefore, its computational cost is more expensive and comparable to that of MD simulations.[1]

X. Liu · S. Li (✉) · N. Sheng
Department of Civil and Environmental Engineering,
University of California, Berkeley, CA 94720, USA
e-mail: shaofan@berkeley.edu

[1] In the rest of the paper, when we use the term "QC method," we refer to the local version of QC method, unless indicated otherwise.

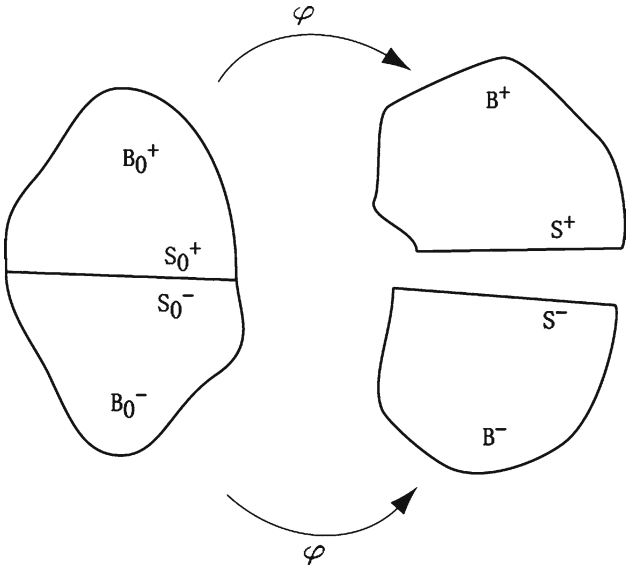

Fig. 1 Illustration of a cohesive surface under finite deformation

A natural question to ask is: *Can we simulate non-uniform local deformation by using the local version of the QC method?* The objective of this work is to use the local QC method to simulate one particular local inhomogeneous deformation: strong discontinuity or surface separation. The main idea of the present approach is to incorporate the cohesive FEM into the local QC framework to form a hybrid cohesive QC-FEM method, which can effectively deal with inhomogeneous local deformations, particularly arbitrary strong discontinuities. In this work, we propose a coarse-grain approach to formulate interfacial cohesive relations solely based on the information along interfaces at the atomic level.

This paper is arranged in the following way. In Sect. 2 we shall present in detail the cohesive QC method, in which a new surface potential based on atomic information is proposed. In Sect. 3 we shall discuss the lattice eigenstrain method and how to apply the eigenstrain method to cohesive QC-FEM. To validate the method, we present a simulation of a screw dislocation propagation in Sect. 4. We then conclude the presentation by making a few remarks in Sect. 5.

2 The cohesive law in a QC

In this section, we consider a solid subjected to an inhomogeneous deformation that is caused by a displacement discontinuity as shown in Fig. 1. In engineering applications, this type of strong discontinuities is the characterization of fracture or dislocations. Initially as a single connected domain, Ω_0, the body is broken into two disjointed pieces. In the referential configuration, the fracture surface, or the plane of division, is denoted as S_0, and it divides the body into two halves: $\Omega_0 = B_0^+ \bigcup B_0^-$. After the deformation $\boldsymbol{\varphi}$,

$$\boldsymbol{\varphi} : \Omega_0 \to \Omega; \tag{1}$$

the body arrives at its deformed or current configuration, Ω (see Fig. 1). We use $\mathbf{x}$ denoting the spatial position of a material point $\mathbf{X}$ at the time t, i.e.

$$\mathbf{x} = \boldsymbol{\varphi}(\mathbf{X}) = \mathbf{u} + \mathbf{X}.$$

Two crack surfaces now move to S^+ and S^-, respectively. And the two deformed halves are denoted by B^+ and B^-. Due to atomic interactions, there will be surface traction between S^+ and S^-. In the rest of the paper, we shall call the fracture surfaces the cohesive surfaces and the surface traction as the cohesive traction.

The strong form of the governing equations of the problem, i.e. the equations of motion, can be written as:

$$\mathrm{DIV}[\mathbf{P}(\boldsymbol{\varphi})] + \rho_0 \mathbf{B} = \rho_0 \ddot{\boldsymbol{\varphi}} \quad \text{in } B_0^{\pm} \tag{2}$$

$$\boldsymbol{\varphi} = \bar{\boldsymbol{\varphi}} \quad \text{on } \partial_{\varphi} B_0 \tag{3}$$

$$\mathbf{P}(\boldsymbol{\varphi}) \cdot \boldsymbol{\mathcal{N}} = \bar{\mathbf{t}} \quad \text{on } \partial_t B_0 \tag{4}$$

$$\mathbf{P}^+ \cdot \boldsymbol{\mathcal{N}}^+ = \mathbf{P}^- \cdot \boldsymbol{\mathcal{N}}^- \quad \text{on } S_0^{\pm} \tag{5}$$

where $\mathbf{B}$ is the body force, ρ_0 is the mass density in referential configuration. In above equations, the symbol DIV is the material divergence operator, i.e. $\nabla_{\mathbf{X}} \cdot$, $\boldsymbol{\mathcal{N}}$ is the normal vector of surfaces including the cohesive surface, $\bar{\mathbf{t}}$ is the prescribed traction on $\partial_t B_0$. It is assumed that the traction is continuous along the cohesive surface, S_0, (5). For domain boundaries, note that

$$\partial_{\phi} B_0 = \partial_{\phi} B_0^+ \bigcup \partial_{\phi} B_0^- \quad \text{and} \quad \partial_t B_0 = \partial_t B_0^+ \bigcup \partial_t B_0^- \tag{6}$$

where $\partial_{\varphi} B$ is the portion of the boundaries where the displacements are prescribed, and $\partial_t B$ is the portion of the boundaries where the traction is prescribed.

In (2)–(5), $\mathbf{P}(\boldsymbol{\varphi})$ is the first Piola–Kirchhoff stress tensor. If we consider the constitutive relation of a hyperelastic material with an elastic energy density W, we may write

$$\mathbf{P} = \frac{\partial W}{\partial \mathbf{F}}$$

which clearly indicates that $\mathbf{P}$ is the function of the deformation map, i.e. $\mathbf{P} = \mathbf{P}(\boldsymbol{\varphi})$.

Via standard procedures, we can then derive the Galerkin weak formulation for Eqs. 2–5:

$$\int_{B_0^{\pm}} \rho_0 \ddot{\boldsymbol{\varphi}} \cdot \delta\boldsymbol{\varphi} dV + \int_{B_0^{\pm}} \mathbf{P}(\boldsymbol{\varphi}) \cdot \delta\mathbf{F} dV = \int_{\partial_t B_0^{\pm}} \bar{\mathbf{t}} \cdot \delta\boldsymbol{\varphi} dS + \int_{S_0} (\mathbf{P}(\boldsymbol{\varphi}) \cdot \mathbf{N}) \cdot \delta(\boldsymbol{\varphi}^+ - \boldsymbol{\varphi}^-) dS \tag{7}$$

The last term in the above equation is the virtual work done by the cohesive traction force across the plane of discontinuity. If we define the jump there as:

$$\boldsymbol{\Delta} = \boldsymbol{\varphi}^+ - \boldsymbol{\varphi}^- \tag{8}$$

then we can re-write the last term as:

$$\int_{S_0} (\mathbf{P}(\boldsymbol{\varphi}) \cdot \boldsymbol{\mathcal{N}}) \cdot \delta(\boldsymbol{\varphi}^+ - \boldsymbol{\varphi}^-) dS = \int_{S_0} \mathbf{t}^{\text{cohe}} \cdot \delta \boldsymbol{\Delta} dS \tag{9}$$

where $\mathbf{t}^{\text{cohe}}$ denotes the cohesive traction. In the continuum cohesive theory e.g. [14], $\mathbf{t}^{\text{cohe}}$ is defined through the cohesive law:

$$\mathbf{t}^{\text{cohe}} = \frac{\partial W^s}{\partial \boldsymbol{\Delta}} \tag{10}$$

where W^s is the surface energy density.

In the continuum cohesive theory, W^s is *empirical*. One has to take extra effort to choose the surface potential, and then justify one's choice. Sometimes we just cannot justify them to accommodate complex size effects. To be true to the spirit of coarse graining, one should be able to derive surface cohesive relations based on the atomic microstructure. However, the difficulty appears to be the discontinuity as a form of local inhomogeneous deformation, which makes the Cauchy–Born rule break down and hence the coarse graining scheme. To resolve this issue, we need to modify the *bulk* Cauchy–Born rule to incorporate or accommodate kinematics of surface separation. In other words, we need a *discontinuous* Cauchy–Born rule, so we can extend the QC formulation to situations where the strong discontinuity or surface separation is present. Before doing so, we first briefly review the procedures of the QC method by deriving the first Piola–Kirchhoff stress $\mathbf{P}$ from atomistic level information.

The basic assumption of the (local) QC method is that within a local region Ω_e the deformation gradient $\mathbf{F} = \mathbf{F}^e$ is constant. In the setting of FE methods, we can view Ω_e as an FE element, most appropriately a triangular element. The energy density W^e is then defined as:

$$W^e = \frac{E^e}{V_e} \tag{11}$$

where E^e is the total energy within Ω_e and V_e is the volume. E^e can be computed by summing the energies for all atoms in Ω_e:

$$E^e = \sum_{i=1}^{N_e} E_i(r^{i1}, r^{i2}, \ldots, r^{iN_e}), \tag{12}$$

and N_e is the total number of atoms in Ω_e, E_i is the energy of atom i and

$$r^{ij} := |\mathbf{x}_i - \mathbf{x}_j|, \quad j = 1, 2, \ldots, N_e$$

are the atomic distances between atoms i and j in the current configuration.

For the local QC method to be a coarse-grained approach, a key assumption on local deformation has to be mandated: that is the so-called Cauchy–Born rule (see [2,3]) It states that, with a constant $\mathbf{F}^e$, all atoms in the underlying lattice within the same element deform the same way, i.e.

$$\mathbf{r}^{ij} = \mathbf{F}^e \mathbf{R}^{ij} \tag{13}$$

Here $\mathbf{r}^{ij} := \mathbf{x}_i - \mathbf{x}_j$ denotes the position vector between atom i and j in the deformed lattice and $\mathbf{R}^{ij} := \mathbf{X}_i - \mathbf{X}_j$ is the difference of the lattice vectors in the original lattice.

With the Cauchy–Born rule, E^e can be simplified as:

$$E^e = N_e E_i(r^{i1}, r^{i2}, \ldots, r^{iN_e}) = N_e E_i(\mathbf{F}^e) \tag{14}$$

where i is the index for the ith atom in Ω_e, which may represent any atom in Ω_e. The energy of the whole domain Ω is then obtained by summing E^e over all elements:

$$E = \sum_{e=1}^{n_{\text{elem}}} E^e \tag{15}$$

where n_{elem} is the total number of elements.

We now derive the expression for $\mathbf{P}^e$, the first Piola–Kirchhoff stress within an element. For simplicity, we only consider the case of two-body interaction. However, the derivations can be extended to multi-body interactions without difficulty. From now on, we shall also drop the suffix e in expressions. One should keep in mind all the quantities are within Ω^e. We first re-write E^e as:

$$E^e = N_e E_i(r^{i1}, r^{i2}, \ldots, r^{iN_e}) = \frac{N_e}{2} \sum_{j=1}^{M_b} E_{ij}(r^{ij}(\mathbf{F})) \tag{16}$$

where E_{ij} is the potential energy between a pair of atoms, i and j, and $1/2$ factor is due to the double counting a pair potential. M_b is the number of atoms interacting with atom i in the bulk material. In general, $M_b \ll N_e$ if we ignore the far-field interactions. $\mathbf{P}$ can be written as:

$$\begin{aligned} \mathbf{P} &= \frac{\partial W^e}{\partial \mathbf{F}} = \frac{N_e}{2V_e} \sum_{j=1}^{M_b} \frac{\partial E_{ij}(r^{ij})(\mathbf{F})}{\partial \mathbf{F}} \\ &= \frac{N_e}{2V_e} \sum_{j=1}^{M_b} E'_{ij}(r^{ij}) \frac{\partial r^{ij}(\mathbf{F})}{\partial \mathbf{F}} \end{aligned} \tag{17}$$

In the above equation, $E'_{ij}(r^{ij}) = \dfrac{dE_{ij}}{dr^{ij}}$ as E_{ij} is a function of a single variable r^{ij}. The quantity $\dfrac{\partial r_{ij}}{\partial \mathbf{F}}$ can be computed as:

$$\frac{\partial r^{ij}(\mathbf{F})}{\partial \mathbf{F}} = \frac{\partial r^{ij}}{\partial \mathbf{r}^{ij}} \frac{\partial \mathbf{r}^{ij}}{\partial \mathbf{F}} = \frac{\mathbf{r}^{ij} \otimes \mathbf{R}^{ij}}{r^{ij}} \tag{18}$$

In deriving the above expression, (13) is used. The final expression of $\mathbf{P}$ reads:

$$\mathbf{P} = \frac{N_e}{2V_e} \sum_{j=1}^{M_b} E'_{ij}(r^{ij}) \frac{\mathbf{r}^{ij} \otimes \mathbf{R}^{ij}}{r^{ij}} \tag{19}$$

The above derivations are not new, and the objective of this work is to use the same philosophy to derive the cohesive traction law for $\mathbf{t}^{\text{cohe}}$ based on the information of lattice structures of the solid. To do so, we have to first express the surface energy density in a surface element W^{es} in terms of atomic potentials. We assume in this paper that W^{es} can be determined solely from the atoms distributed along the pair of cohesive surfaces. This assumption is similar to the nearest-neighbor-interaction assumption, and it can be lifted at the cost of more involved calculations.

We now consider a pair of opposite crack surface element S^{se+} and S^{se-}. They are the edges of two FE elements. Since we only need to formulate W_e^s for one of the edges, without losing generality, we shall only consider S^{se+}. The surface energy density is defined as:

$$W^{es} = \frac{E^{es}}{A_{es}} \tag{20}$$

where E^{es} is the total surface energy within the surface element S^{se+}, and A_{es} is the surface area. For E^{es}, we have:

$$E^{es} = \sum_{i=1}^{N_{es}} E_i^s \tag{21}$$

where N_{es} is the number of atoms within the surface element S^{se+} and

$$E_i^s = \frac{1}{2}\sum_{j=1}^{M_s} E_{ij}(r_s^{ij}) \tag{22}$$

where $E_{ij}(r_s^{ij})$ are atomistic potentials for surface atoms, r_s^{ij} are interatomic distances across the interface, i and j are indices for surface atoms only, and M_s is the number of atoms on the opposite surface element S^{se-} that interact with atom i on the surface element S^{se+}.

Remark 1 1. It assumes that the interface atomic distance, $r_s^{ij} = r_s^{ij}(\boldsymbol{\Delta}_d)$, is not a function of the local deformation gradient $\mathbf{F}$, but the nodal displacement separation (the jump) of associated surface elements. For simplicity, in the rest of paper, we drop the subscript, $_s$, unless it is important to indicate it. The nodal displacement separation is constant within each element. Therefore, this is essentially *an interface Cauchy–Born rule*, and we should further elaborate this point later.

2. In calculating atomistic surface energy potential, as a preliminary study, we only consider the nearest neighbor interaction, and hence the effect of long-range interactions such as surface relaxation is neglected. Moreover, this lack of physical realism can be fixed, for instance, by using a so-called surface Cauchy–Born approach ([15]). In fact, the procedure proposed by [15] is one way to calculate atomic surface potentials. It may be possible that we can still use the proposed approach, but choose an appropriate surface potential, $E_{ij}^{\mathcal{S}}(r^{ij}) \neq E_{ij}(r^{ij})$, to capture some of surface effects. In fact, there have been some specific surface potentials proposed in the literature, e.g. [7].

Similar to what we did for element interior, we adopt the following QC approximation:

$$E^{es} \approx N_{es} E_i^s \tag{23}$$

where N_{es} is the number of atoms on the surface element S^{se+}. This approximation means that we assume that all atoms in S^{se+} to have the same surface energy.

To derive the expression for the cohesive traction, we consider a FE discretization of the domain. The FE approximation of the displacement field is given by:

$$\mathbf{u}(\mathbf{X}) = \mathbf{N}(\mathbf{X})\mathbf{d} \tag{24}$$

where

$$\mathbf{N}(\mathbf{X}) = [N_{ij}(\mathbf{X})]^{n_{\text{dim}} \times n_{\text{dof}}}$$

is the shape function matrix, n_{dim} is the number of dimension of space, n_{dof} is the number of degrees of freedom, and $\mathbf{d}$ is the nodal displacement vector. In the following, we shall mix the tensor notation with matrix notation in the derivation, because some of the matrices here may be viewed as second-order tensors.

Consider a separation, or a jump, between a pair of cohesive surfaces as shown in Fig. 2. The jump can also be described by FEM interpolation:

$$\boldsymbol{\Delta} = \mathbf{N}^s(\mathbf{X})\boldsymbol{\Delta}^d \tag{25}$$

where $\mathbf{N}^s(\mathbf{X})$ is the matrix of edge shape functions. The nodal jump vector $\boldsymbol{\Delta}^d$ is defined by:

$$\boldsymbol{\Delta}^d = \mathbf{d}^+ - \mathbf{d}^- \tag{26}$$

where $\mathbf{d}^+$ and $\mathbf{d}^-$ are nodal displacement vectors on S^+ and S^-, respectively. Moreover, the following relationship holds:

$$\mathbf{d}^+ = \langle \mathbf{d} \rangle + \frac{1}{2}\boldsymbol{\Delta}^d \tag{27}$$

$$\mathbf{d}^- = \langle \mathbf{d} \rangle - \frac{1}{2}\boldsymbol{\Delta}^d \tag{28}$$

where $\langle \mathbf{d} \rangle = \frac{1}{2}(\mathbf{d}^+ + \mathbf{d}^-)$. So,

$$\frac{\partial \mathbf{d}^+}{\partial \boldsymbol{\Delta}^d} = \frac{1}{2} \tag{29}$$

$$\frac{\partial \mathbf{d}^-}{\partial \boldsymbol{\Delta}^d} = -\frac{1}{2} \tag{30}$$

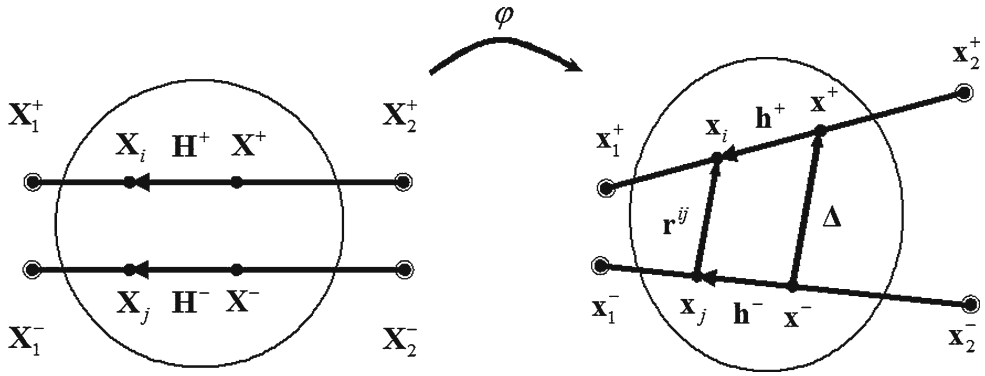

Fig. 2 Interface kinematics: the bond separation between between two cohesive surfaces

In the discrete case, the virtual work done by the cohesive force can be re-written as:

$$\int_{S_0} \mathbf{t}^{\text{cohe}} \cdot \delta \boldsymbol{\Delta} dS = \int_{S_0} \frac{\partial W^s}{\partial \boldsymbol{\Delta}^d} \cdot \delta \boldsymbol{\Delta}^d dS = \int_{S_0} \frac{\partial W^s}{\partial \boldsymbol{\Delta}^d} \cdot \delta \mathbf{d}^+ dS - \int_{S_0} \frac{\partial W^s}{\partial \boldsymbol{\Delta}^d} \cdot \delta \mathbf{d}^- dS \tag{31}$$

We can define the global *nodal* cohesive traction vector array from the above equation:

$$\mathbf{f}^{\text{cohe}} = \int_{S_0} \frac{\partial W^s}{\partial \boldsymbol{\Delta}^d} [\mathbf{N}^S]^T dS \tag{32}$$

where $[\mathbf{N}^S]$ is the global surface edge shape function matrix.

In computations, the quantity $\dfrac{\partial W^s}{\partial \boldsymbol{\Delta}^d}$ is calculated first at the element level. We first assume that in each element e there are $es = 1, \ldots, n_{\text{selem}}$ cohesive interfaces. Then in an element,

$$W^s = \sum_{es=1}^{n_{\text{selem}}} W^{es} H(S_0^{es})$$

where $H(S_0^{es})$ is the characteristic function or support function of the surface element S_0^{es}, i.e.

$$H(S_0^{es}) = \begin{cases} 1 & \mathbf{X} \in S_0^{es} \\ 0 & \mathbf{X} \notin S_0^{es} \end{cases}$$

Then for a given cohesive interface, es,

$$\frac{\partial W^{es}}{\partial \boldsymbol{\Delta}^d} = \frac{N_{es}}{2A_{es}} \sum_{j=1}^{M_s} E'_{ij}(r^{ij}) \frac{\partial r^{ij}}{\partial \boldsymbol{\Delta}^d} = \frac{N_{se}}{2A_{es}} \sum_{j=1}^{M_s} E'_{ij}(r^{ij}) \frac{\mathbf{r}^{ij}}{r^{ij}} \frac{\partial \mathbf{r}^{ij}}{\partial \boldsymbol{\Delta}^d} \tag{33}$$

In order to calculate $\dfrac{\partial \mathbf{r}^{ij}}{\partial \boldsymbol{\Delta}^d}$, we need to establish *an interfacial kinematics* to represent local inhomogeneous deformation due to surface separation.

Refer to Fig. 2 for the following discussion. For a an arbitrary point $\mathbf{X}$ on the cohesive surface the jump is defined as $\boldsymbol{\Delta}(\mathbf{X})$. Since the jump is actually the stretch or separation of two adjacent atomic planes, the representative point $\mathbf{X}$ are in fact two points $\mathbf{X}^{\pm}$ in the reference configuration. Their images in deformed configuration are the points $\mathbf{x}^+$ and $\mathbf{x}^-$. However, in the QC description, we view them as the *same* reference point in the QC description.

A spatial point at atomic scale is not physically meaningful, if there is no atom residing at the point. So to define the jump at an arbitrary location needs a material point for reference. We use a pair of adjacent atoms $\mathbf{x}_i \in S^{se+}$ and $\mathbf{x}_j \in S^{se-}$ and the related the local position vectors $\mathbf{h}^+$ and $\mathbf{h}^-$ to locate $\mathbf{x}^{\pm}$, i.e.

$$\mathbf{x}^+ = \mathbf{x}_i - \mathbf{h}^+, \quad \text{and} \quad \mathbf{x}^- = \mathbf{x}_j - \mathbf{h}^-.$$

which are the spatial difference between the atoms on $S^{se\pm}$ and the spatial representative points $\mathbf{x}^{\pm}$. Note that physically points $\mathbf{x}^+$ and $\mathbf{x}^-$ come from reference points $\mathbf{X}^+$ and $\mathbf{X}^-$, which are apart at an equilibrium atomic distance, $\mathbf{R}$.

With this local kinematic setup, we can express the bond separation in terms of FEM nodal displacement separation. We start from the following geometric condition (see Fig. 2),

$$\mathbf{r}^{ij} = \boldsymbol{\Delta} + \mathbf{h}^+ - \mathbf{h}^- \tag{34}$$

Here $\boldsymbol{\Delta}$ is the jump at the point $\mathbf{X}$, where we want to evaluate $\dfrac{\partial \mathbf{r}^{ij}}{\partial \boldsymbol{\Delta}^d}$. We can view $\mathbf{X}$ as positions of Gauss quadrature points that are needed to evaluate integrations in (31). Since elements in each half of the deformed body obey the Cauchy–Born rule, $\mathbf{h}^+$ and $\mathbf{h}^-$ can be written as:

$$\mathbf{h}^+ = \mathbf{F}^+ \mathbf{H}^+ \tag{35}$$

$$\mathbf{h}^- = \mathbf{F}^- \mathbf{H}^- \tag{36}$$

where $\mathbf{F}^+$ and $\mathbf{F}^-$ are local deformation gradients at different halves of the body and $\mathbf{H}^+$ and $\mathbf{H}^-$ are local interatomic

position vectors in the undeformed configuration corresponding to the spatial position vectors, $\mathbf{h}^{\pm}$. The above equations can then be re-written as:

$$\mathbf{h}^{\pm} = \mathbf{F}^{\pm}\mathbf{H}^{\pm} = \left(\mathbf{1} + \mathbf{u}^{\pm}_{,\mathbf{X}}\right) \cdot \mathbf{H}^{\pm} = \mathbf{1} \cdot \mathbf{H}^{\pm} + \mathbf{B}^{\pm} \cdot \left(\mathbf{d}^{\pm} \otimes \mathbf{H}^{\pm}\right) \tag{37}$$

where $\mathbf{B}^{\pm}$ are two third-order tensors whose components are defined as

$$B^{\pm}_{ijA} = N^{\pm}_{ij,A} := \frac{\partial}{\partial X_A} N^{\pm}_{ij} \tag{38}$$

Here the capital letter A denotes the index of the reference coordinates.

Considering the interfacial kinematic relation shown in Fig. 2, we have the following geometric relations at an arbitrary point (a pair of points) of the interface,

$$\begin{aligned} \boldsymbol{\Delta} &= \mathbf{r}^{ij} + (\mathbf{h}^{-} - \mathbf{h}^{+}) = (\mathbf{x}_i - \mathbf{x}_j) + (\mathbf{h}^{-} - \mathbf{h}^{+}) \\ &= \mathbf{F}^{+} \cdot \mathbf{X}_i - \mathbf{F}^{-} \cdot \mathbf{X}_j + \mathbf{F}^{-} \cdot \mathbf{H}^{-} - \mathbf{F}^{+} \cdot \mathbf{H}^{+} \\ &= \mathbf{F}^{+} \cdot \mathbf{X}^{+} - \mathbf{F}^{-} \cdot \mathbf{X}^{-} \end{aligned} \tag{39}$$

Define

$$\bar{\mathbf{X}} := \frac{1}{2}\left(\mathbf{X}^{+} + \mathbf{X}^{-}\right), \quad \text{and} \quad \boldsymbol{\Delta}_0 := \frac{1}{2}\left(\mathbf{X}^{+} - \mathbf{X}^{-}\right). \tag{40}$$

We have *the interface Cauchy–Born rule* as follows:

$$\boxed{\boldsymbol{\Delta} = \left(\mathbf{F}^{+} + \mathbf{F}^{-}\right) \cdot \boldsymbol{\Delta}_0 + \left(\mathbf{F}^{+} - \mathbf{F}^{-}\right) \cdot \bar{\mathbf{X}}} \tag{41}$$

Now, we can calculate the derivative of $\mathbf{r}^{ij}$ with respect to element nodal jump vector, $\boldsymbol{\Delta}^d$,

$$\begin{aligned} \frac{\partial \mathbf{r}^{ij}}{\partial \boldsymbol{\Delta}^d} &= \frac{\partial \boldsymbol{\Delta}}{\partial \boldsymbol{\Delta}^d} + \frac{\partial \mathbf{h}^{+}}{\partial \boldsymbol{\Delta}^d} - \frac{\partial \mathbf{h}^{-}}{\partial \boldsymbol{\Delta}^d} \\ &= \mathbf{N}^s + \frac{\partial \mathbf{h}^{+}}{\partial \mathbf{d}^{+}} \frac{\partial \mathbf{d}^{+}}{\partial \boldsymbol{\Delta}^d} - \frac{\partial \mathbf{h}^{-}}{\partial \mathbf{d}^{-}} \frac{\partial \mathbf{d}^{-}}{\partial \boldsymbol{\Delta}^d} \\ &= \mathbf{N}^s + \frac{1}{2}\mathbf{B}^{+}\mathbf{H}^{+} - \frac{1}{2}\mathbf{B}^{-}\mathbf{H}^{-} \end{aligned} \tag{42}$$

The final expression of $\dfrac{\partial W^{es}}{\partial \boldsymbol{\Delta}^d}$ reads:

$$\begin{aligned} \frac{\partial W^{es}}{\partial \boldsymbol{\Delta}^d} &= \frac{N_{es}}{2A_{es}} \sum_{j=1}^{M_s} E'_{ij}(r^{ij}) \frac{\partial r^{ij}}{\partial \boldsymbol{\Delta}^d} \\ &= \frac{N_{es}}{2A_{es}} \sum_{j=1}^{M_s} E'_{ij}(r^{ij}) \frac{1}{r^{ij}} \left(\mathbf{r}^{ij} \cdot \mathbf{N}^s + \frac{1}{2}\mathbf{r}^{ij} \cdot \mathbf{B}^{+}\mathbf{H}^{+} - \frac{1}{2}\mathbf{r}^{ij} \cdot \mathbf{B}^{-}\mathbf{H}^{-}\right) \end{aligned} \tag{43}$$

The matrix form of the above equation is:

$$\frac{\partial W^{es}}{\partial \boldsymbol{\Delta}^d} = \frac{N_{es}}{2A_{es}} \sum_{j=1}^{M_s} \frac{E'_{ij}(r^{ij})}{r^{ij}} \left([\mathbf{N}^{sT}]\mathbf{r}^{ij} + \frac{1}{2}[\mathbf{B}^{+}\mathbf{H}^{+}]^T \mathbf{r}^{ij} - \frac{1}{2}[\mathbf{B}^{-}\mathbf{H}^{-}]^T \mathbf{r}^{ij}\right) \tag{44}$$

The components of matrices $\mathbf{B}^{\pm}\mathbf{H}^{\pm}$ are:

$$[\mathbf{B}^{\pm}\mathbf{H}^{\pm}]_{ij} = N^{\pm}_{ij,A} H^{\pm}_{A} \tag{45}$$

where $N^{\pm}_{ij}$ are components of $\mathbf{N}$. The force vector $\mathbf{f}^{\text{cohe}}$ can be obtained by integrating $\dfrac{\partial W^s}{\partial \boldsymbol{\Delta}^d}$.

Remark 2 From (43), we observe that when $\mathbf{B}^{+}\mathbf{H}^{+} = \mathbf{B}^{-}\mathbf{H}^{-}$, the expression of nodal traction vector will reduce to:

$$\mathbf{f}^{\text{cohe}} = \mathop{\mathop{A}_{e=1}^{n_{\text{elem}}} \mathop{A}_{es=1}^{n_{\text{selem}}}}_{S_0^{es}} \int \frac{N_{es}}{2A_{es}} \sum_{j=1}^{M_s} \frac{E'_{ij}(r^{ij})}{r^{ij}} \mathbf{N}^{sT} \mathbf{r}^{ij} dS \tag{46}$$

This corresponds to the case when the deformed atomic position vectors are the same on S^{+} and S^{-}. In the above equation $\boldsymbol{A}$ is the element assembly operator for both bulk elements and surface elements [6]. Since in each element there may be several cohesive interfaces, i.e. $es = 1, \ldots, n_{\text{selem}}$, so we have used double assembly operators as a two-loop assembly for each bulk element and for each surface element within a bulk element.

In Fig. 3, we plot $\mathbf{f}^{\text{cohe}}$ against $\boldsymbol{\Delta}^d$. Of the two nodes, we shall plot $\mathbf{f}^{\text{cohe}}_1$. The two edges are chosen to be parallel to each other, so $\boldsymbol{\Delta}^d_1 = \boldsymbol{\Delta}^d_2 = \boldsymbol{\Delta}$. The interatomic distance is 1 and the edge length is 10. The Lennard–Jones (LJ) potential is used. The expression for E_{ij} is:

$$E_{ij}(r^{ij}) = 4\epsilon \left[\left(\frac{\sigma}{r^{ij}}\right)^{12} - \left(\frac{\sigma}{r^{ij}}\right)^{6}\right] \tag{47}$$

with $\sigma = \epsilon = 1$. When plotting Fig. 3a, we fix Δ_t, i.e. the tangential component of $\boldsymbol{\Delta}$ is set to zero, and vary Δ_n, the normal component of $\boldsymbol{\Delta}$, which means that in this case the node on S^{+} is aligned longitudinally with a node on S^{-}. When plotting Fig. 3b, we fix $\Delta_n = -1$ and vary Δ_t. It is observed that as expected the normal traction shows a similar pattern as the interatomic force and the tangential traction has a period of the lattice constant. In both figures we show different cases when we include nearest neighbor only, up to the 2nd nearest neighbor, and up to the 3rd nearest neighbor. One can find that while the nearest neighbor interaction is good enough for the normal traction, it yields a jump for the tangential traction when the node is in the middle of two atoms. The jump happens because with nearest neighbor interaction, the moving node "switches" its interacting partner in the middle and the force changes its sign. This

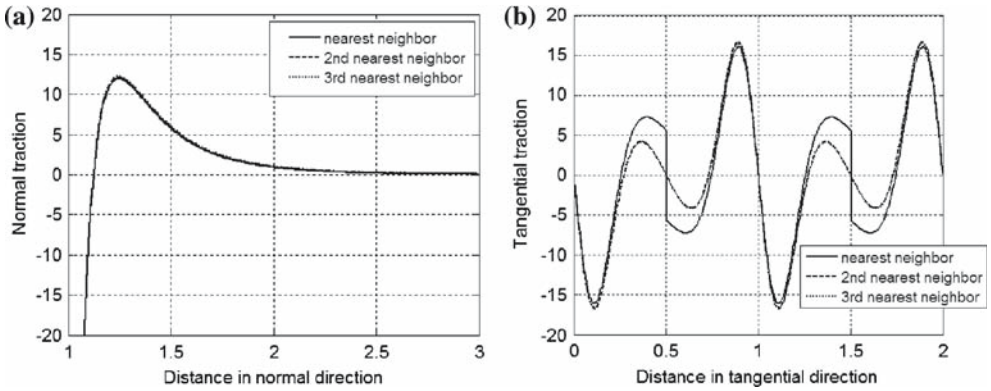

Fig. 3 Cohesive traction as a function of distances. **a** Normal traction, and **b** Tangential traction

artificial effect is eliminated when the 2nd nearest neighbor interaction is considered. [17] provided a similarly shaped cohesive relation by using an empirical surface potential.

The other terms in the weak form can be treated by standard FE procedures, and we choose not to show the derivation. The final expression is:

$$\mathbf{M}\ddot{\mathbf{d}} + \mathbf{f}^{int}(\mathbf{d}) - \mathbf{f}^{\text{cohe}}(\mathbf{d}) = \mathbf{f}^{\text{ext}} \tag{48}$$

where:

$$\mathbf{M} = \overset{n_{\text{elem}}}{\underset{e=1}{\mathbf{A}}} \int_{B_0^e} \rho_0 \mathbf{N}^{eT}\mathbf{N}^e dV \tag{49}$$

$$\mathbf{f}^{int} = \overset{n_{\text{elem}}}{\underset{e=1}{\mathbf{A}}} \int_{B_0^e} \mathbf{B}^{eT}\mathbf{P}^e(\mathbf{d}) dV \tag{50}$$

$$\mathbf{f}^{\text{ext}} = \overset{n_{\text{elem}}}{\underset{e=1}{\mathbf{A}}} \int_{\partial_t B_0^{\pm e}} \mathbf{N}^{eT}\bar{\mathbf{t}}^e dS \tag{51}$$

and $\mathbf{B}^e$ is the matrix for element shape function gradient.

3 Application in simulation of dislocation propagations

In general, a line defect like the dislocation will naturally occur when a crystal is under external stress. When the configurational force i.e. the Peach-Koehler force is greater than the lattice friction force i.e. the Peierls force under specific temperature, the dislocation will then move.

There are many techniques in Molecular Dynamics to simulate dislocation motions. To study the motion of a single dislocation, there are even analytical solutions as well as semi-analytical solutions available for Molecular Dynamics or Lattice Dynamics. The analytical approach was first developed for Lattice Statics by [11], and it was then extended by [13] to Lattice Dynamics. In analytical solution procedure, the dislocation is preconfigured, and the Lattice Green's Function technique is often used to solve dislocation motions. This technique can only be employed in an infinite lattice space. For finite lattice spaces, the semi-analytical solution is useful. In the semi-analytical solution, the dislocation is preconfigured, i.e. the defect field is initially prescribed by imposing a so-called eigenstrain field, the MD simulation then takes care of the rest based on the equation of motion or the interatomic force relation. This type of solutions is very suitable to serve as the benchmark solution for numerical simulations because of their analytical nature.

Here, we briefly outline this method first, and then compare its results to that of the proposed cohesive QC-FEM computation. We consider a general 3D lattice, and we limit ourselves to the case of harmonic approximation. For an atom ℓ, the equation of motion reads:

$$m_a\ddot{\mathbf{u}}(\ell) = -\sum_{\ell'} \boldsymbol{\phi}(\ell, \ell')\mathbf{u}(\ell') \tag{52}$$

where m_a is the mass, $\boldsymbol{\phi}(\ell, \ell')$ is the coefficient of a constant matrix that is related to the force between atoms ℓ and ℓ'. Furthermore, we have the following expression:

$$\mathbf{u}(\ell') - \mathbf{u}(\ell) = \left[\boldsymbol{\beta}(\ell, \ell') + \boldsymbol{\beta}^*(\ell, \ell')\right]\mathbf{x}(\ell'\ell) \tag{53}$$

where $\mathbf{x}(\ell'\ell) = \mathbf{x}(\ell') - \mathbf{x}(\ell)$. $\boldsymbol{\beta}(\ell, \ell')$ and $\boldsymbol{\beta}^*(\ell, \ell')$ are the elastic distortion and the eigen-distortion between ℓ and ℓ', respectively. We have a non-zero eigen-distortion if the domain is subject to inelastic deformations like dislocations.

Remark 3 The symmetric part of (53) is analogous to the following equation in the theory for continuum:

$$\frac{1}{2}\left(\nabla\mathbf{u} + (\nabla\mathbf{u})^T\right) = \boldsymbol{\epsilon}^e + \boldsymbol{\epsilon}^* \tag{54}$$

where $\boldsymbol{\epsilon}^e$ is the elastic strain and $\boldsymbol{\epsilon}^*$ is the eigenstrain.

Mura [13] showed that with (53), the MD equation of motion takes a new form:

$$m_a\ddot{\mathbf{u}}(\ell) = -\sum_{\ell'} \boldsymbol{\phi}(\ell, \ell')\mathbf{u}(\ell') + \sum_{\ell'} \boldsymbol{\phi}(\ell, \ell')\boldsymbol{\beta}^*(\ell, \ell')\mathbf{x}(\ell\ell') \tag{55}$$

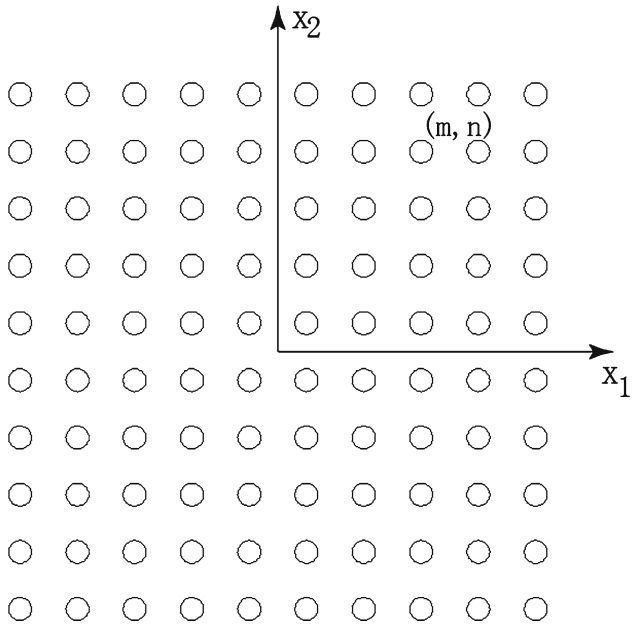

Fig. 4 A plane view of the cubic lattice

The extra term on the right hand side (55) is a fictitious body force due to eigen-distortions which are caused by defects.

Now let us consider the a specific type of defects: a screw dislocation. We shall use it as an example to illustrate how the value of the dislocation force is calculated by eigen-strains. The problem setting is shown in Fig. 4. We consider a cubic lattice with nearest neighbor interactions. An index pair (m, n) is used to denote a particular atom. The interatomic distance is h. The screw dislocation is in the x_3-direction and is moving in the x_1-direction with a constant speed v. As a result, we only need to consider x_3-direction displacements.

Let us assume the dislocation has propagated to the column of atoms with $m = m_0$. Then for all pair of atoms $(k+0.5, -0.5)$ and $(k+0.5, 0.5), k \in (-\infty, m_0]$, the inelastic displacement is h, i.e. the amount of dislocation. So we have:

$$\beta^*(\ell, \ell')x_2(\ell'\ell) = h \tag{56}$$

Since $x_2(\ell'\ell) = h$, we have $\beta^* = 1$ in this case. Thus it is easy to obtain the following equation of motion [8]:

$$\begin{aligned} m_a\ddot{u}_3(m,n) = {} & A\left[u_3(m+1,n)+u_3(m-1,n)\right] \\ & +B\left[u_3(m,n+1)+u_3(m,n-1)\right] \\ & -2(A+B)u_3(m,n) \\ & +Bh\sum_{k=-\infty}^{m_0}\left(\delta_{m,k+0.5}\delta_{n,0.5}-\delta_{m,k-0.5}\delta_{n,-0.5}\right) \end{aligned} \tag{57}$$

where A and B are force constants in x_1x_3- and x_2x_3-directions, respectively. By applying the above procedure to Molecular Dynamics, we can simulate dislocation motions in a lattice.

In our cohesive QC-FEM approach, the dislocation forces $\pm Bh$ are treated as prescribed forces. For FE nodes that are at and behind the dislocation front, we apply the dislocation forces. They appear in the external force vector $\mathbf{f}^{\text{ext}}$. To propagate the dislocation, we adopt the so-called quarter-jump rule [11]. Let $\mathbf{x}^+$ and $\mathbf{x}^-$ be two atoms locating at the opposite sides of the dislocation plane. If the following condition is satisfied:

$$\Delta = u_3(\mathbf{x}^+) - u_3(\mathbf{x}^-) > 0.25h \tag{58}$$

we consider the dislocation having passed through this point, and we start to apply dislocation forces to the adjacent pair of nodes.

4 A numerical example

In this section, we present the numerical simulation of a propagating screw dislocation using the cohesive QC-FEM approach. We simulate a domain with a dimension of $[-50, 50] \times [-50, 50]$. The interatomic spacing is chosen to be 1. The force constants are $A = B = 1$. The dislocation initiates at the left side of the domain. We performed two simulations. One has 200 linear triangle elements and the other one has 800 elements. The cohesive surface is chosen to be the $x = 0$ plane. For comparison purpose, we also simulate the problem with Molecular Dynamics(MD). The equation of motion is (57). There are total of 10201 atoms.

For time integration, Verlet algorithm is used in both cases. The time steps are 0.3162 and 0.1581 for the cohesive QC-FEM simulations and 0.0316 for the MD simulation.

The simulations were carried out in a PC with an 1.8 GHz AMD64 processor. The different CPU times used in computations of the same problem but with different modelings and different discretizations are tabulated in Table 1. From Table 1, one may find that the cohesive QC-FEM simulation has far less computational cost than that of the MD simulation: the 200-element simulation and the 800-element simulation take 0.7 and 5.5% of the time of MD simulation, respectively. At the same time, the cohesive QC-FEM simulation still has a very good accuracy. Shown in Figs. 5 and 6 are the displacement profiles at time $t = 6.3240$ and $t = 12.6480$. We can see the cohesive QC-FEM simulation captures the main feature of the problem. Table 2 shows the dislocation speed (computed by the distance that the dislocation front has traveled by time). We observe that dislocation speed is close between the results obtained by the cohesive QC-FEM and by MD. It should be noted that since the computation is done for fictitious materials the unit for the dislocation speed here is used a computational unit that has not

Table 1 Comparison of the running time between cohesive QC-FEM and MD simulations

	QC (200 elements)	QC (800 elements)	MD
Running time (s) ($t = 6.3240$)	0.7340	5.4680	98.7500
Running time (s) ($t = 12.6480$)	1.3440	10.6410	195.9220

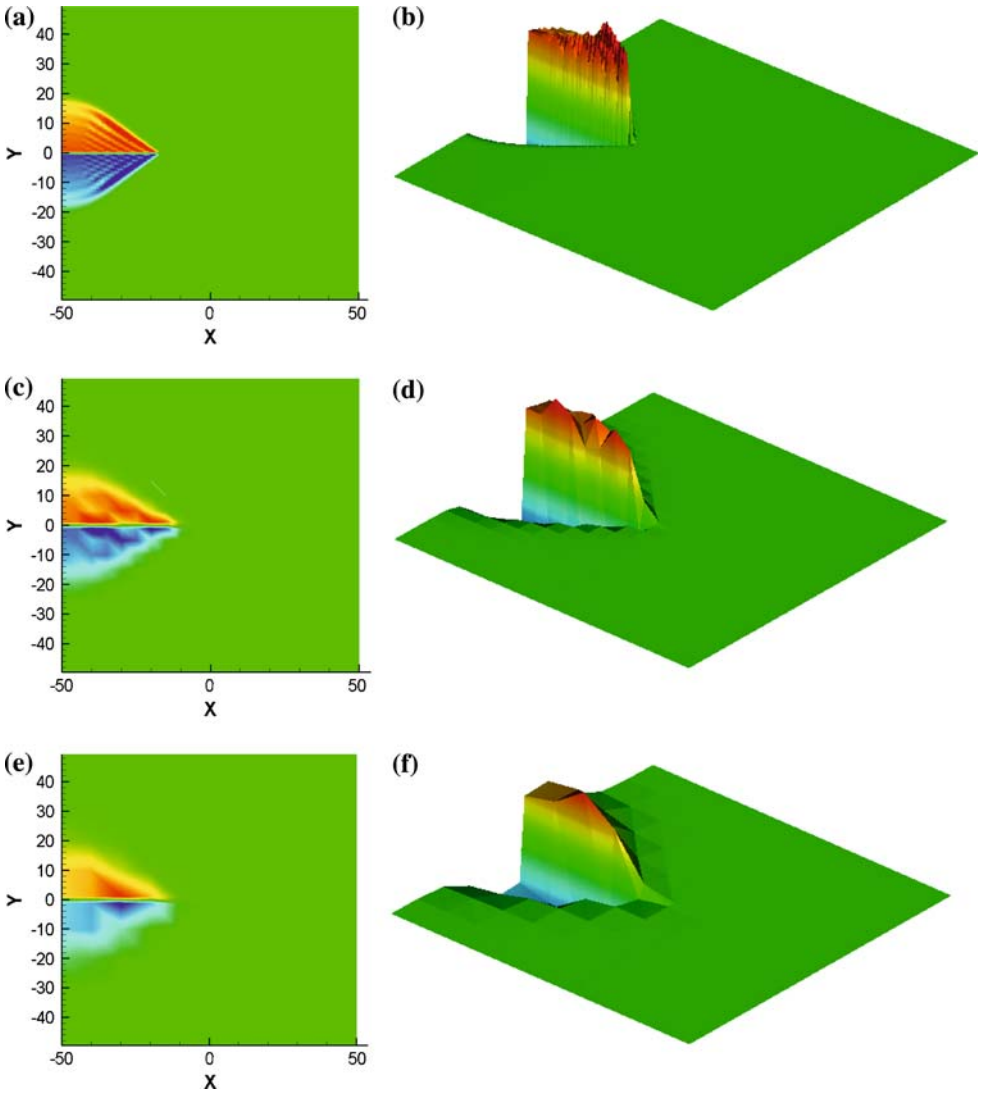

Fig. 5 Displacement profiles at $t = 6.3240$. **a, b** MD results. **c, d** Cohesive QC-FEM results with 800 elements. **e, f** are cohesive QC-FEM results with 200 elements

been converted to SI system. Nevertheless, the comparison itself is meaningful.

One of the main concerns of cohesive finite element method is its mesh-dependence. To test mesh dependence for the proposed cohesive QC-FEM, we have carried out calculations in three different meshes, i.e. $n_{\text{elem}} = 200, 800,$ and 3,200. We choose the dislocation speed as the physical index to measure mesh dependency, and the results are tabulated in Table 2 in comparison with that of molecular dynamics simulation. From Table 2, one may find that as the mesh is refined, the dislocation speed obtained in cohesive QC-FEM approaches to that of MD simulation. Indeed, the numerical simulation results are dependent on mesh size, and it is possible that it depends on mesh orientation as well,[2] but as QC-FEM mesh is refined towards to the resolution of the underlying lattice structure, we expect the results of the cohesive QC-FEM simulation will converge to the results of MD simulation.

This example demonstrates that if other details of a moving dislocation are not the primary concern than the moving dislocation itself, the cohesive QC-FEM method may be a very good choice in the simulation of dislocation motions because of its efficiency and cost-effectiveness.

[2] We shall test that case in a separated study.

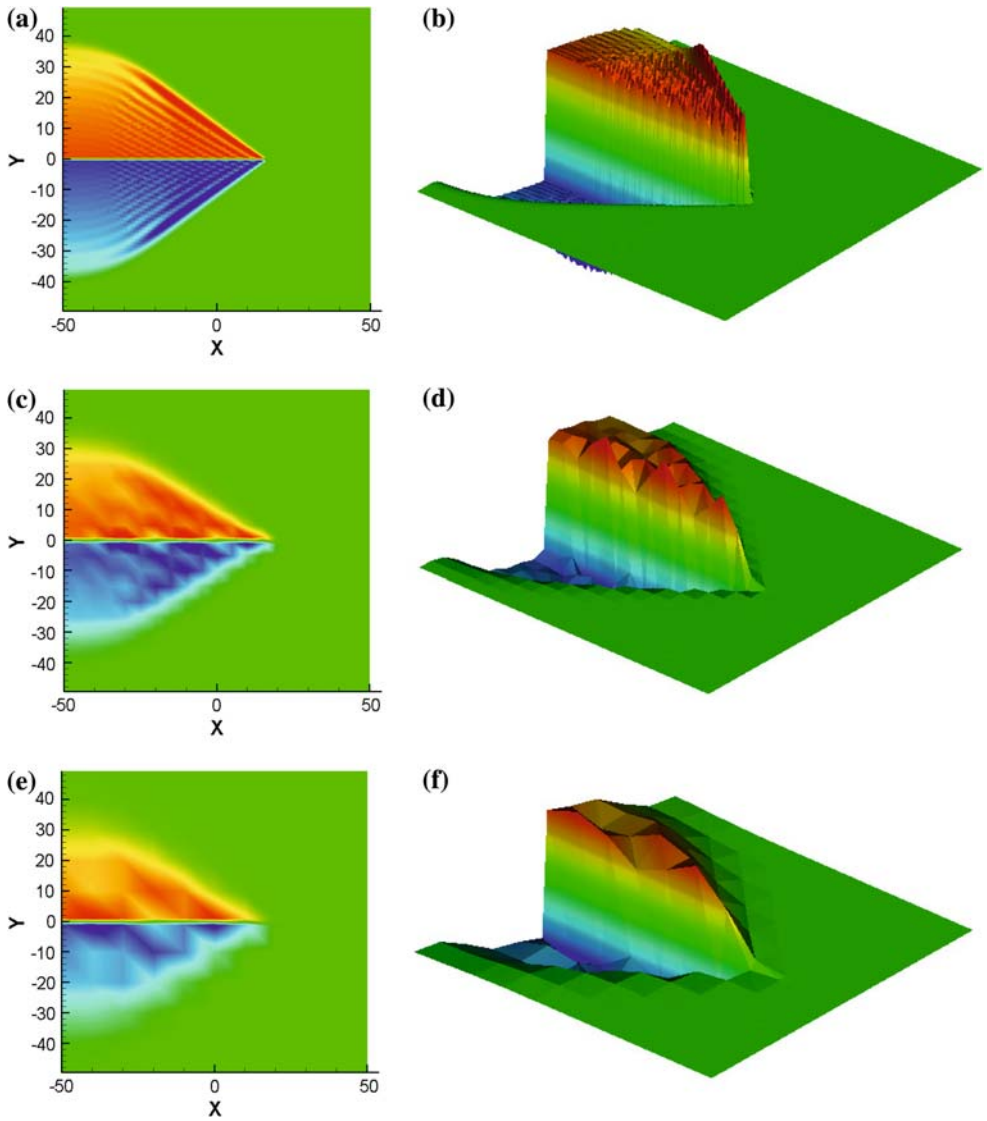

Fig. 6 Displacement profiles at $t = 12.6480$. **a, b** MD results. **c, d** The cohesive QC-FEM results with 800 elements. **e, f** The cohesive QC-FEM results with 200 elements

Table 2 Comparison of the dislocation speed between cohesive QC-FEM and MD simulations

	QC (200 elements)	QC (800 elements)	QC (3,200 elements)	MD
Dislocation speed				
Measured at $t = 6.3240$ s	6.325	5.534	5.139	5.218
Dislocation speed				
Measured at $t = 12.6480$ s	5.534	5.139	5.337	5.297

5 Conclusions

A cohesive QC FEM is formulated. It is capable of dealing with strong continuities across a solid at nano-scale, such as micro-cracks and dislocations. Compared to the conventional cohesive FEM, the proposed method takes a new path by exploiting atomistic information to construct the cohesive law. By doing so, the QC formulations extend from the interior of the solid to the interfaces, and it is more accurate then macroscale empirical approaches. Utilizing the technique of the eigenstrain technique, we use the proposed method to simulate a moving screw dislocation. The numerical results show that the proposed method has good accuracy and computational efficiency.

We are currently working on extending the method to 3D problems and problems involving with multiple dislocations. By using the atomic information, the proposed method can also be incorporated into a multiscale scheme with the molecular dynamics method. This has recently been done by the present authors [10]. A multiscale simulation of a moving screw dislocation has been carried out there, which allows a dislocation passing through different scales. In short, we believed that the proposed method provides an effective coarse grained approach to simulate fracture and dislocation motions.

Acknowledgments The authors acknowledge the fact that Mr. Ashutosh Agrawal participated the early phase of this work. We thank him for his suggestion of using a spring model to represent surface cohesive law and his early involvement in computer code development. This work is supported by a grant from NSF (Grant no. CMS-0239130), which is greatly appreciated.

References

1. Belytschko T, Moës N, Usui S, Parimi C (2001) Arbitrary discontinuities in finite elements. Int J Numer Methods Eng 50:993–1013
2. Born M (1915) Dynamik der Krystallgitter. Teubner, Leipzid/Berlin
3. Born M, Huang K (1954) Dynamical theory of crystal lattices. Clarendon Press, Oxford
4. Callari C, Armero F (2004) Analysis and numerical simulation of strong discontinuities in finite strain poroplasticity. Comput Methods Appl Mech Eng 193:2941–2986
5. Dolbow J (1999) An extended finite element method with discontinuous enrichment for applied mechanics. PhD Thesis, Northwestern University
6. Hughes TJR (1987) The finite element method: linear static and dynamic finite element analysis. Prentice Hall, Englewood Cliffs
7. Ibach H (1997) The role of surface stress in reconstruction, epitaxial growth and stabilization of mesoscopic structures. Surf Sci Rep 29:193–263
8. King KC, Mura T (1991) The eigenstrain method for small defects in a lattice. J Phys Chem Solids 52:1019–1030
9. Klein P, Gao H (1998) Crack nucleation and growth as strain localization in a virtual bond continuum. Eng Fract Mech 61:21–48
10. Li S, Liu X, Agrawal A, To AC (2006) The perfectly matched multiscale simulations for discrete systems: Extension to multiple dimensions. Phys Rev B 74:045418
11. Maradudin A (1958) Screw dislocations and discrete elastic theory. J Phys Chem Solids 9:1–20
12. Miller RE, Tadmor EB (2002) The quasicontinuum method: overview, applications and current directions. J Comput Aided Materials Des 9:203–239
13. Mura T (1977) Eigenstrains in lattice theory. University of Waterloo Press, Waterloo
14. Ortiz M, Pandolfi A (1999) Finite-deformation irreversible cohesive elements for three-dimensional crack-propagation analysis. Int J Numer Methods Eng 44:1267–1282
15. Park H, Klein P, Wagner G (2006) A surface Cauchy–Born model for nanoscale materials. Int J Numer Methods Eng 68:1072–1095
16. Tadmor E, Ortiz M, Phillips R (1996) Quasicontinuum analysis of defects in solids. Philos Mag A 73:1529–1563
17. Xu X-P, Needleman A (1994) Numerical simulations of fast crack growth in brittle solids. J Mech Phys Solids 42:1397–1434